Two distinct ballistic processes in graphene at the Dirac point

M. Lewkowicz,[1] B. Rosenstein,[2,3,1,*] and D. Nghiem[2]
[1]*Physics Department, Ariel University Center of Samaria, Ariel 40700, Israel*
[2]*Electrophysics Department, National Chiao Tung University, Hsinchu 30050, Taiwan, Republic of China*
[3]*National Center for Theoretical Sciences, Hsinchu 30043, Taiwan, Republic of China*
(Received 7 July 2011; published 15 September 2011)

The dynamical approach is applied to ballistic transport in mesoscopic graphene samples of length L and contact potential U. At times shorter than both relevant time scales, the flight time $t_L = L/v_g$ (v_g is Fermi velocity) and $t_U = \hbar/U$, the major effect of the electric field is to create electron-hole pairs, i.e., causing interband transitions. In linear response, this leads (for width $W \gg L$) to conductivity $\sigma_2 = \pi/2\ e^2/h$. On the other hand, at times lager than the two scales, the mechanism and value are different. It is shown that the conductivity approaches its intraband value, equal to the one obtained within the Landauer-Bütticker approach resulting from evanescent waves. It is equal to $\sigma_1 = 4/\pi\ e^2/h$ for $W \gg L$ and $t_U \ll t_L$. The interband transitions, within linear response, are unimportant in this limit. Between these extremes there is a crossover behavior dependent on the ratio between the two time scales t_L/t_U. At strong electric fields (beyond linear response) the interband process dominates. The electron-hole mechanism is universal, namely, does not depend on geometry (aspect ratio, topology of boundary conditions, properties of leads), while the evanescent modes mechanism depends on all of them. On basis of the results we determine that while in absorption measurements and in dc transport in suspended graphene σ_2 was measured, σ_1 would appear in experiments on small ballistic graphene flakes on substrate.

DOI: 10.1103/PhysRevB.84.115419 PACS number(s): 72.80.Vp, 81.05.ue, 73.23.Ad, 05.60.Gg

I. INTRODUCTION

Electronic mobility in graphene, especially one suspended on leads, is extremely large,[1] so that a graphene sheet is one of the purest electronic systems. The relaxation time of charge carriers due to scattering of impurities, phonons, ripplons, etc., in suspended graphene samples of submicron length is so large that the transport is ballistic.[2,3] The ballistic flight time in these samples can be estimated as

$$t_L = L/v_g\,, \tag{1}$$

where $v_g \simeq 10^6$ m/s is the graphene velocity characterizing the massless "ultrarelativistic" spectrum of graphene near the Dirac points, $\varepsilon_k = v_g|\mathbf{k}|$, and L is the length of the sample that can exceed several μm.[4] The extraordinary physics appears right at the Dirac point at which the density of states vanishes. In particular, at this point graphene exhibits a quasi-Ohmic behavior, $\mathbf{J} = \sigma\mathbf{E}$, even in the purely ballistic regime.

Determination of the value of the minimal dc conductivity at Dirac point in the limit of zero temperature has undergone a period of experimental and theoretical uncertainty. Early on its value $\sigma \simeq 4e^2/h$ was measured in graphene on a substrate,[5] yet consequently, it was shown in experiments on suspended samples[2] that the zero-temperature limit was not achieved, and that, in fact, these early samples had too many charged "puddles," so that they represented an average around the neutrality point. The value in early suspended samples[2] was half of that and most recently settled around third of this value in the best samples at 2 K temperature.[4] Theoretically, several different values for the dc conductivity appeared. The value

$$\sigma_1 = \frac{4}{\pi}\frac{e^2}{h} \tag{2}$$

had been considered as the "standard" one for several years,[6,7] and appeared as a zero-disorder limit of the self-consistent harmonic approximation.[8] It was derived for the infinite sample and this implies the assumption that the potential difference U at the contacts between the metallic leads and the graphene flake is unimportant (this is currently under intensive experimental[9] and theoretical[10–13] investigation). An alternative and independent approach to ballistic transport in mesoscopic graphene samples[14] of finite length L with a large contact barrier U was pioneered in Ref. 15 following ideas in Ref. 16. They applied the Landauer-Büttiker formula for conductance derived for transport in (quasi) one-dimensional channels.

The value

$$\sigma_2 = \frac{\pi}{2}\frac{e^2}{h} \tag{3}$$

was obtained in the dynamical approach to an infinite sample[17] and is equal to the ac value calculated under the condition $\omega \gg T/\hbar$ at finite temperatures,[18–20] while other values, like $\sigma_3 = 4\frac{e^2}{h}$, also appeared in the literature.[21] The dynamical approach to transport was applied to the tight-binding model of graphene[17] to resolve this "regularization ambiguity." The ballistic evolution of the current density in time after a sudden or gradual switching on of the electric field E was evaluated and approaches the large-times limit $\sigma_2 E$. The physical nature of the quasi-Ohmic "resistivity" without either charge carriers or dissipation in infinite samples (namely, neglecting leads or "reservoir") is as follows.[17,22] The electric field creates electron-hole excitations in the vicinity of the Dirac points similar to the Landau-Zener tunneling effect in narrow-gap semiconductors[23] or electron-positron pair creation in quantum electrodynamics.[24,25] Importantly, in graphene, the energy gap is zero, thus the pair creation is possible at zero temperature and arbitrary small $\mathbf{E}$, even within linear response. Although the absolute value of the quasiparticle velocity v_g cannot be altered by the electric field due to the "ultrarelativistic" disper-

sion relation, the orientation of the velocity can be influenced by the applied field.The electric current, $e\mathbf{v}$, proportional to the projection of the velocity $\mathbf{v}$ onto the direction of the electric field, is increased by the field. These two sources of current, namely, creation of moving charges by the electric field (polarization) and their reorientation (acceleration), are responsible for the creation of a stable current.[17,22,26] The result within linear response is that the current settles very fast, on the microscopic time scale of $t_\gamma = \hbar/\gamma \simeq 0.24$ fs (γ being the hopping energy), on the asymptotic value.

A deeper analysis of the "quasi-Ohmic" graphene system beyond the leading order in perturbation theory in electric field revealed[27] that on the time scale

$$t_{\rm nl} = \sqrt{\frac{\hbar}{eEv_g}}, \tag{4}$$

the linear response breaks down due to intensive Landau-Zener-Schwinger's (LZS) pair creation and leads to a linear increase with time.[28] At times larger than $t_{\rm nl}$, the result is consistent with the WKB approximation.[26,29] This is in contrast to dissipative systems in which the linear response limit can be taken directly at infinite time. This perhaps is the origin of the "regularization" ambiguities in graphene, since large-time and small-field limits are different. Recently, the WKB approximation to the interband or the LZS transition was extended to the finite samples.[30] In this case, the ballistic evolution is "truncated" at ballistic time t_L, see Eq. (1). It is (sometimes implicitly) assumed, within both the dynamical approach and the Kubo approach, that there is no significant contact barrier U between the leads and the graphene flake.

In contrast, the Landauer-Büttiker (LB) approach hinges on the description of the leads in terms of a potential energy barrier of a certain nonzero barrier height $U(r)$.[10] The first quantized Weyl equation therefore was considered in Ref. 15 in full analogy to the one-particle Schrödinger equation to define the T matrix and it was found, surprisingly, that quasi-Ohmic behavior emerges for large aspect ratios, $W/L \to \infty$, and, moreover, the conductivity is precisely σ_1 for rectangular samples. The approach was extended to barriers of various shapes,[31] boundary conditions,[11] and nonrectangular geometries like Corbino disks using conformal mapping.[32] It was established that the conductance is quite sensitive to the topology of the sample, but rather insensitive to the potential shape. This approach cannot be extended to the ac fields. This is an additional motivation to extend the dynamical approach to include the effects of the barrier potential. The barrier potential provides an additional time scale

$$t_U = \hbar/U. \tag{5}$$

It looks like the physical picture behind the LB approach is almost "orthogonal" to the one of the ultrarelativistic pair creation mentioned above. In this paper, we rigorously apply the dynamical approach to study transport in mesoscopic samples. We demonstrate that the physics behind the two values of the dc conductivity is quite different despite the fact that numerically $\sigma_2 = 1.57e^2/h$ is just 24% higher than $\sigma_1 = 1.27e^2/h$ for the stripe geometry (this is quite accidental due to the nonuniversality of the latter value[32]). A recent numerical simulation of the dynamics of a graphene ribbon[33] demonstrates that the value of conductance corresponding to σ_2 on a short time scale crosses over at t_L (via a series of strong oscillations) into one corresponding to the LB conductance in the ribbon (analogous to σ_1) at asymptotically long times. These two physical processes governing the ballistic transport are quite distinct. One is fast and homogeneous: the interband channel (valence and conduction "cones" of graphene near Dirac point), namely, the electron-hole creation sometimes referred to (usually beyond linear response) as Landau-Zener tunneling, or, in particle physics, the Schwinger's pair creation.[34] It is unique to graphene (and some other systems with similar band structure like topological insulators) and has certain surprising features. For example, this channel of conduction "dries out" or is depleted for any finite sample. The second mechanism, the intraband transition, despite constituting a peculiar "relativistic" kind of electron acceleration, is much more common. It is important for transport only for a sufficiently large contact potential between the leads and the graphene sample and unlike the interband channel, is a long-time phenomenon.

We use the dynamical approach to determine what process is dominant for the evolution of the I-V curve of a finite graphene sample directly at the neutrality point, with the contact barrier taken into account. We explore this evolution on different time scales t, which can be associated with the frequency $\omega \sim 1/t$ for a periodic pulse or the pulse duration in the relaxation-type experiments.[35,36] The physics depends essentially on the relation of a time scale t with respect to the three physical time scales t_L, t_U, and $t_{\rm nl}$ defined above in Eqs. (1), (5), and (4). It is demonstrated analytically that for a finite barrier potential and finite length, the infinite-time limit coincides in linear response with a generalization of the LB calculation in Ref. 15. The results are summarized in Table I.

In more detail, in Sec. II we start from the definition of a model neglecting effects of the contact potential barrier, namely for $t_U \gg t_L, t_{\rm nl}$. The dynamical approach to ballistic transport in the infinite sample is briefly outlined (this way, σ_2 is obtained). The approach is generalized to the case of a finite sample and the decay of the interband channel is demonstrated. In Sec. III, a phenomenological model of the graphene-lead coupling is specified and certain stationary properties, like the quasi-one- particle T matrix, are constructed. The LB results are slightly generalized to the case of an arbitrary barrier height U equal to the chemical potential of the leads. It will be interpreted as a long-time limit of the intraband contribution within the dynamical approach to the finite sample formulated in Sec. IV. The evolution of the current in graphene at a Dirac point for an arbitrary potential barrier is given here (within linear response) as an integral. Results of the numerical evaluation of the integral together with the

TABLE I. The long-time limit of the conductivity in a graphene flake for various sample and experimental parameter ratios.

t_L/t_U	t_L/t_{nl}	dominant process	conductivity σ	kind of response
$\ll 1$	$\ll 1$	interband	σ_2 Eq. (3)	linear
$\ll 1$	$\gg 1$	interband	Eq. (19)	nonlinear
$\gg 1$	$\gg 1$	intraband	σ_1 Eq. (45)	linear

analytically obtained short- and the long-time asymptotes are given in Secs. V and VI for the intraband and the interband contributions, respectively. The results are summarized and discussed in Sec. VI.

II. SMALL CONTACT BARRIER: DYNAMICAL APPROACH TO THE INTERBAND TRANSITION

A. The Hamiltonian for the infinite sample

The electrons in a constant and homogeneous electric field near the "right helicity" Dirac point[6] are approximately described by the Weyl Hamiltonian:

$$\hat{H} = \hat{K} + \hat{V}, \tag{6}$$

$$\hat{K} = \int d^2r\ \hat{\psi}_r^\dagger K \hat{\psi}_r, \quad K = -i\hbar v_g \boldsymbol{\sigma}\cdot\boldsymbol{\nabla}, \tag{7}$$

$$\hat{V} = e\int d^2r\ \hat{\psi}_r^\dagger V \hat{\psi}_r, \quad V = \frac{\hbar v_g}{c}\boldsymbol{\sigma}\cdot\mathbf{A} + \Phi, \tag{8}$$

where K and V are first quantized operators and the annihilation operator $\hat{\psi}_r^\alpha$ is a two-component $\alpha = 1,2$ (pseudo) spinor. $\mathbf{A}$ and Φ are the vector and the scalar potentials describing the electric field, which is switched on at $t = 0$, oriented along the y axis and, importantly, is coordinate independent. We employ units in which $\hbar = v_g = 1$. In momentum basis, $\hat{\psi}_\mathbf{r} = \frac{1}{\sqrt{WD}}\sum_\mathbf{k} e^{i\mathbf{k}\cdot\mathbf{r}}\hat{\psi}_\mathbf{k}$, where D is an infrared cutoff and W is the width that also will be treated as large. When the constant electric field is written in a gauge that respects the translational symmetry, $\Phi = 0$, $\mathbf{A} = (0, -cEt)$, the different momenta decouple:

$$\hat{H} = \sum_\mathbf{k} \hat{\psi}_\mathbf{k}^\dagger \boldsymbol{\sigma}\cdot\left(\mathbf{k} + \frac{e}{c}\mathbf{A}\right)\hat{\psi}_\mathbf{k}. \tag{9}$$

The model is a rather crude idealization of the experimental situation in several respects. The sample is considered "infinite" and absolutely homogeneous. This allows a convenient use of the axial gauge invariant under translations. Finite width (perpendicular to the electric field) generally creates no complications and the whole discussion can be repeated for a finite W and a variety of boundary conditions. On the other hand, finite length L breaks the translational invariance and simplicity is lost; this is one of the subjects of the present paper. The second idealization pertains the description of leads. It is assumed that the leads are absolutely unintrusive, namely, one can imagine the Corbino disk geometry or a lead with no contact potential difference. The more general case, with a potential barrier, will be treated below.

The spectrum before the electric field is switched on is divided into positive and negative energy parts describing the valence and conduction band:

$$(\boldsymbol{\sigma}\cdot\mathbf{k})u_\mathbf{k} = -\varepsilon_\mathbf{k} u_\mathbf{k}, \quad (\boldsymbol{\sigma}\cdot\mathbf{k})v_\mathbf{k} = \varepsilon_\mathbf{k} v_\mathbf{k}, \tag{10}$$

$$u_\mathbf{k} = \frac{1}{\sqrt{2}}\begin{pmatrix}1\\ -z_\mathbf{k}\end{pmatrix}, \quad v_\mathbf{k} = \frac{1}{\sqrt{2}}\begin{pmatrix}1\\ z_\mathbf{k}\end{pmatrix}, \tag{11}$$

where $z_\mathbf{k} = (k_x + ik_y)/\varepsilon_\mathbf{k}$ is a phase and $\varepsilon_\mathbf{k} = |\mathbf{k}|$. Since all the momenta are independent in the Hamiltonian (9) due to use of the gauge in which the electric field is represented via a homogeneous vector potential, a second quantized state is uniquely characterized by the "first quantized" amplitude:

$$\psi_\mathbf{k}(t) = \begin{pmatrix}\psi_\mathbf{k}^1(t)\\ \psi_\mathbf{k}^2(t)\end{pmatrix}, \tag{12}$$

which is a "spinor" in the sublattice space. It obeys the matrix Schrödinger equation in sublattice space: $i\partial_t\psi_\mathbf{k} = \boldsymbol{\sigma}\cdot(\mathbf{k} + \frac{e}{c}\mathbf{A})\psi_\mathbf{k}$. The initial condition corresponding to a second quantized state at zero temperature in which all the negative energy states are occupied and all the positive energy states are empty is $\psi_\mathbf{k}(t = 0) = u_\mathbf{k}$.

The evolution of the current density, $\hat{\mathbf{J}} = -4e\hat{\psi}_r^\dagger\boldsymbol{\sigma}\hat{\psi}_r$, of a state in terms of this amplitude is

$$j_y(t) = -4e\sum_{\mathbf{k}:\varepsilon_\mathbf{k}<\mu} \psi_\mathbf{k}^\dagger(t)\sigma_y\psi_\mathbf{k}(t). \tag{13}$$

The factor four is due to spin and valley degeneracies of the Weyl fermions. To leading order in the dc electric field for $\mu = 0$ one obtains[17] $\sigma = \sigma_2$, Eq. (3). The same result is obtained for any frequency.[19,20] It was calculated analytically in the tight-binding model for arbitrary E (beyond linear response) in Ref. 28. Corrections to both dc and ac conductivities were computed in Ref. 27 and reveal that the linear response breaks down at $t_{\rm nl}$ as mentioned above and is perhaps a source of the "regularization ambiguity" in linear response. The dynamical approach provides a simple interpretation for the nature of the excitations: the copious creation of electron-hole pairs or interband transitions. Beyond linear response these transitions can be treated either within the Landau-Zener (or WKB) approximation[25,26,30] or exactly by using Schwinger's method.[27]

The simple method of calculation used in the above works hinges on the translational invariance of both the sample and the electric field. However, as long as the electric field is treated within linear response only, one may also consider an inhomogeneous bias. It turns out that in graphene at Dirac point, if there is no potential barrier like the one assumed within the LB approach (and discussed in detail below), the current density decays with time even as the local electric field stays constant.

B. Linear response: decay of the current in a finite sample with a finite range of the electric field

To model the bias voltage, we assume that the electric field is homogeneous in the segment $-L/2 < y < L/2$, and therefore can be described by a scalar potential:

$$\Phi(y) = \frac{V_0}{2}\begin{cases}1, & \text{for } y < -L/2,\\ -2y/L, & \text{for } -L/2 < y < L/2,\\ -1, & \text{for } L/2 < y,\end{cases} \tag{14}$$

(and $\mathbf{A} = 0$), see the dashed line in Fig. 1. This assumption holds even in high-current experimental situations like the one described in Ref. 30. The current, to leading order in perturbation $\hat{V}$, Eq. (8), for the Dirac point, $U_{\rm gate} = 0$, is

$$I_y(t) = -4W\sum_{\mathbf{l},\mathbf{p}} \frac{1 - e^{-i(\varepsilon_\mathbf{p}+\varepsilon_\mathbf{l})t}}{\varepsilon_\mathbf{p} + \varepsilon_\mathbf{l}} \langle u_\mathbf{l}|\hat{V}|v_\mathbf{p}\rangle\langle v_\mathbf{p}|\hat{J}_y|u_\mathbf{l}\rangle + \text{c.c.} \tag{15}$$

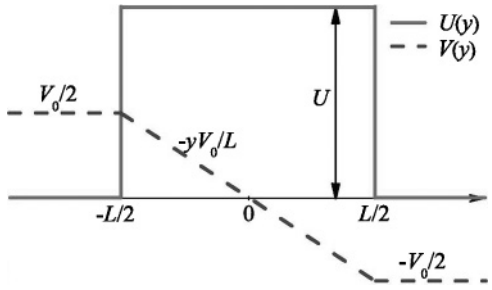

FIG. 1. (Color online) The potential energy barrier $U(y)$ (green line) describes the contact of the leads with the sample, while the bias electric potential $V(y)$ (blue dashed line) describes the applied constant electric field (from $-L/2$ to $L/2$).

As explained in detail in Sec. IV of Ref. 27, the current within the Weyl model has an ultraviolet divergence that should be removed in a chirally invariant manner. Since the present case is not different in this respect from that of the infinite range electric field, the details are omitted. After some algebra, the conductance (for large W, so that continuum momentum can be used) takes the form

$$G(t) = \frac{We^2}{\pi^3 L}\int_{k=-\infty}^{\infty}\int_{p,l=0}^{\infty} \times \frac{\sin[(p-l)L/2](l\varepsilon_{kp} - p\varepsilon_{kl})}{(p-l)^2\varepsilon_{kl}\varepsilon_{kp}}\frac{\sin[t(\varepsilon_{kp}+\varepsilon_{kl})]}{\varepsilon_{kp}+\varepsilon_{kl}}, \tag{16}$$

where $k = l_x = p_x$, $l = l_y$, $p = p_y$. In terms of dimensionless variables $\bar{\epsilon} = (\varepsilon_{kp} + \varepsilon_{kl})L$, $\delta = L(\varepsilon_{kp} - \varepsilon_{kl})/\bar{\epsilon}$, $\Delta = L(p - l)/\bar{\epsilon}$, one obtains the (effective) scaled conductivity $\sigma(\bar{t}) \equiv G(t)L/W$ as a function of time in units of the flight time $\bar{t} = t/t_L$:

$$\sigma(\bar{t}) = -\frac{4e^2}{\pi^3}\int_{\bar{\epsilon}=0}^{\infty}\frac{\sin(\bar{t}\bar{\epsilon})}{\bar{\epsilon}}\int_{\delta=0}^{1}\int_{\Delta=\delta}^{1} \times \frac{1}{\Delta^3}\sqrt{\frac{\Delta^2-\delta^2}{1-\Delta^2}}\sin\left(\frac{\bar{\epsilon}\Delta}{2}\right). \tag{17}$$

This function is given as the red line in Fig. 2 and has the following behavior. Before $\bar{t} = 1/2$, $\sigma(\bar{t}) = e^2/4$; therefore in physical units one recovers the "dynamical" value $\sigma_2 = \frac{\pi}{2}\frac{e^2}{h} = \frac{e^2}{4\hbar}$. This is just the result of pseudorelativistic invariance (maximal velocity v_g) of the Weyl model. The effect of the finite extent of the electric field has no time to propagate to the center of the sample where the current is defined. Then the current drops fast and settles at t_L into a power decrease

$$\sigma(\bar{t}) = \frac{e^2 L}{4\pi t} = \sigma_2\frac{1}{\pi\bar{t}}. \tag{18}$$

In the whole range $\bar{t} > 1/2$, there is an excellent fit for this function:

$$\sigma(\bar{t}) = \sigma_2\frac{1}{\pi\bar{t} - \pi/2 + 1 - \sqrt{\bar{t}/2 - 1/4}}. \tag{19}$$

Until now the linear response approximation was used. Hence, for a finite range of the electric field (finite distance between the electrodes) a stationary flow state is only possible beyond linear response. The LZS tunneling over the band gap is generally a nonperturbative phenomenon. The linear response is only useful in a limited time, $t < t_{\rm nl}$, due to the ultrarelativistic spectrum of graphene.[28] The interband processes beyond $t_{\rm nl}$ are discussed next.

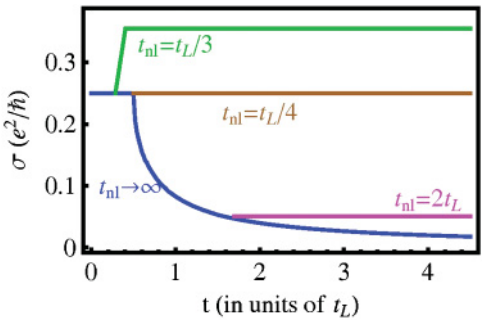

FIG. 2. (Color online) Evolution of the scaled conductivity, Eqs. (3), (19), and (27) at Dirac point for a finite-range electric field (and no contact barrier). The electric field strength determines the time scale $t_{\rm nl}$, Eq. (4), at which nonlinear effects set in.

C. The LZS conductance beyond linear response

Since there are two characteristic times beyond linear response, t_L and $t_{\rm nl}$, three possibilities exist: $t_L \gg t_{\rm nl}$, $t_L \ll t_{\rm nl}$, or $t_L \sim t_{\rm nl}$. In most transport experiments, the ratio $t_L/t_{nl} = L\sqrt{eE/\hbar v_g}$ is smaller than one. The time scale on which nonlinear effects become dominant is not always very large; for example, for experiments not necessarily dedicated to large current transport measurements[37] in which $E = 10^4$ V/m and $L = 0.3$ μm, nonlinearity sets in at $t_{\rm nl} = 0.3$ ps, which is of order of the ballistic time. Moreover, graphene flakes under large fields of order 2×10^6 V/m have been recently studied in specially designed high-current-density experiments.[30] For a sample length $L = 2$ μm, this results in a very large ratio $t_L/t_{\rm nl} = 100$. Therefore it is of importance to calculate the conductance for arbitrary $t_L/t_{\rm nl}$. We start from large fields for which the LZS tunneling is the most effective.

1. $t_L \gg t_{\rm nl}$

Analytic and numerical solutions of the tight-binding model[28] as well as of the Weyl model describing the physics near the Dirac point demonstrated[26,27] that at $t_{\rm nl}$, the creation of electron-hole pairs becomes dominant and is well described by an adaptation of the well-known Schwinger electron-positron pair creation rate $\frac{d}{dt}N \propto (eE)^{3/2}$. The difference with the original derivation[34] in the context of particle physics is that the fermions are $2+1$ dimensional and "massless," thus magnifying the effect. The polarization current is $J(t) = -2ev_g N(t)$ and therefore Schwinger's creation rate at asymptotically long times leads to a linear increase with time:

$$\sigma(t) = \sigma_2(eE)^{1/2}t. \tag{20}$$

Interestingly, this formula is very accurate already at $t = t_{\rm nl}$, see Ref. 28.

The physics of pair creation is highly nonperturbative and nonlinear in nature and therefore, instead of the linear response, Schwinger had to use functional methods to get an exact asymptotic formula. The rate can be intuitively

understood using the much simpler instanton approach originally proposed in the context of particle physics[25] (extended later to low dimensions[24]), that is known in condensed matter physics as the Landau-Zener tunneling probability.[26,30,38]

The density in the infinite sample, calculated using the simple Landau-Zener creation rate expression for one of the flavors, is[25,26]

$$N_{\mathbf{k}}(t) = \Theta(k_y)\Theta(eEt - k_y)\exp\left(-\pi k_x^2/eE\right), \qquad (21)$$

where Θ are the Heaviside functions. One considers the "tunneling" from the conduction band to the valence band at fixed k_x. The gap is given by $2|k_x|$. Consequently, the number of pairs is

$$N(t) = \frac{4}{(2\pi)^2}\int_{\mathbf{k}} N_{\mathbf{k}}(t) = \frac{4}{\pi^2}(eE)^{3/2}t, \qquad (22)$$

corresponding to the Schwinger's pair creation rate $\frac{d}{dt}N = \frac{4}{\pi^2}(eE)^{3/2}$. There is a simple relation within the Weyl model between the rate and the current density, as was shown recently[26] (see also Ref. 24):

$$J = \frac{2e}{\pi^2}\int_{\mathbf{k}}\left[\frac{eEt - k_y}{\sqrt{k_x^2 + (eEt - k_y)^2}}N_{\mathbf{k}}(t) + \frac{\sqrt{k_x^2 + (eEt - k_y)^2}}{eE}\frac{d}{dt}N_{\mathbf{k}}(t)\right]. \qquad (23)$$

Substituting Eq. (21), one obtains

$$J(t) = \frac{2e}{\pi^2}\int_{k_x=0}^{\infty}\left[\sqrt{k_x^2 + (eEt)^2} + k_x\right]\exp\left(-\frac{\pi k_x^2}{eE}\right). \qquad (24)$$

At large t, one arrives at conductivity (20).

Adaptation of the instanton approach to a finite-length sample is quite cumbersome, however, the long-time limit is simple, as was shown in Ref. 30. The range of integration over momenta is determined by the semiclassical condition for tunneling:

$$J(t\to\infty) = \frac{2e}{\pi^2}\int_{k_x=0}^{eEL/2}\int_{k_y=0}^{k_y^{\max}}\frac{k_y}{\varepsilon_{\mathbf{k}}}\exp\left(-\frac{\pi k_x^2}{eE}\right), \qquad (25)$$

where $k_y^{\max} = \sqrt{(eEL)^2 - k_x^2}$. The result for conductivity,

$$\sigma(t\to\infty) = \frac{2e^2}{\pi^3}\left[\frac{\pi L}{2}\sqrt{eE}\ \mathrm{erf}\left(\frac{L}{2}\sqrt{\pi eE}\right) + \exp\left(-\frac{\pi eEL^2}{4}\right) - 1\right], \qquad (26)$$

is presented as a green line in Fig. 2. For $t_L \gg t_{\mathrm{nl}}$, it is proportional to the ratio t_L/t_{nl}:

$$\sigma(t\to\infty) = \frac{e^2L}{\pi^2}\sqrt{eE} = \frac{4}{\pi^2}\sigma_2\frac{t_L}{t_{\mathrm{nl}}}. \qquad (27)$$

This is larger than σ_2 for $t_L/t_{\mathrm{nl}} > \pi^2/4 \approx 2.5$. For these fields, the slow decrease due to finite extent of electric field, L, does not materialize and increases monotonically as function of time t (physically representing the pulse period or pulse duration). For small ratios t_L/t_{nl}, the situation is different.

2. $t_L \ll t_{\mathrm{nl}}$

In the case of small electric fields, one first encounters at t_L a powerwise drop in the current density from the short time value σ_2 as in Eq. (18) before the nonlinear effects take over. For large times $t > t_{\mathrm{nl}}$, one can use the same semiclassical LZ method to determine how the powerwise decrease is halted. The asymptotic value given by Eq. (27) in this case simplifies to

$$\sigma(t\to\infty) = \frac{2e^2}{\pi^2}(eE)L^2 = \frac{8}{\pi^2}\sigma_2\left(\frac{t_L}{t_{\mathrm{nl}}}\right)^2. \qquad (28)$$

This intercept with the slow decreasing current, Eq. (18), see Fig. 2, occurs at very large time $t = \frac{\pi}{8}\frac{t_{\mathrm{nl}}^2}{t_L}$. When t_L is of the same order as t_{nl}, the effective conductivity is approximately σ_2, see values close to $t_L/t_{\mathrm{nl}} = \pi^2/4$. Untill now we neglected the influence of a potential barrier between the leads and graphene on the ballistic transport.

III. CONTACT BARRIER: STATIONARY PROPERTIES AND THE FIRST QUANTIZED LANDAUER-BÜTTIKER APPROACH

A. Phenomenological description of contacts. Symmetry of the Hamiltonian.

One models the effect of coupling to leads by a finite (and sometimes very large[15]) potential energy barrier (that should in principle be found self consistently[10]). The simplest model is the square barrier, see Fig. 1,

$$U(y) = \begin{cases} 0, & \text{for } y > L/2 \text{ or } y < -L/2, \\ U > 0, & \text{for } -L/2 < y < L/2. \end{cases} \qquad (29)$$

The derivation of the model from a microscopic Hamiltonian is discussed in several works, see for example Ref. 10, and it was found to describe a typical transport experiment quite well.

The second quantized Hamiltonian is $\hat{H} = \hat{K} + \hat{V}$, with the perturbation (bias) given in Eq. (8) and the modified "large" part

$$\hat{K} = \int_r \hat{\psi}_r^\dagger H_{1Q}\hat{\psi}_r. \qquad (30)$$

The "first quantized" operator H_{1Q} now contains the barrier potential $U(r)$:

$$H_{1Q} = -i\sigma\cdot\nabla + U(y). \qquad (31)$$

The barrier breaks the translational symmetry, however, for the simple form of the symmetric barrier that we have adopted, Eq. (29), the operator H_{1Q} is invariant under reflection, $P: y\to -y$, supplemented by the spinor rotation,

$$S = P\sigma_x, \quad [H_{1Q}, S] = 0. \qquad (32)$$

The bias potential, Eq. (14), is also chosen to be antisymmetric, which simplifies the considerations.

The presence of a barrier renders the problem analogous to that in mesoscopic physics[23] and suggests that the T matrix approach to transport is useful in this case.

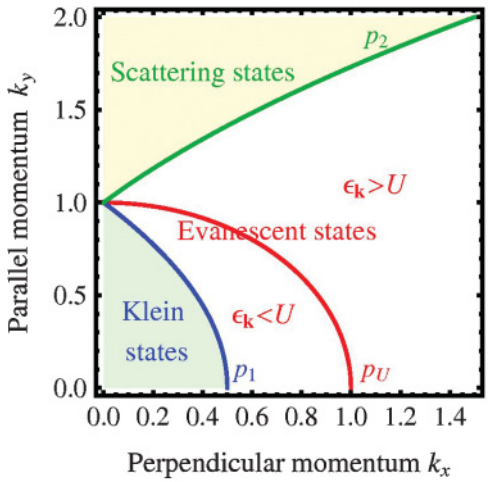

FIG. 3. (Color online) Kinematics of scattering states of the first quantized Weyl equation with a potential barrier. The red line corresponds to $p,l = \sqrt{U^2 - k^2}$, the green to $p,l = \sqrt{U\,(U + 2k)}$, and the blue to $p,l = \sqrt{U\,(U - 2k)}$. The lines separate kinematical regions for the intraband transitions. Here, $U = 1$.

B. T matrix

The LB approach utilizes the notion of a transmission coefficient through the channel n, $T_n \equiv |t_n(\mu)|^2$, where t_n is its amplitude. The conductance is

$$G(\mu) = \frac{e^2}{h} \sum_n T_n, \tag{33}$$

where the summation is over all the open channels. Therefore one should solve the "classical" Weyl equation with a barrier

$$H_{1Q}\psi = [-i\sigma \cdot \nabla + U(y)]\,\psi = \varepsilon\psi. \tag{34}$$

For simplicity, we consider only periodic boundary conditions in the direction perpendicular to the field with "perimeter" W, although various more realistic boundary conditions were discussed in Ref. 15 and numerous works since. Due to translational symmetry in the direction perpendicular to the barrier, we consider a fixed value of the momentum $p_x \equiv k = \frac{2\pi}{W} n_x$. Despite the lack of translational symmetry in the field direction y due to the barrier, one can still use the momentum $p_y \equiv p$ as a good quantum number for scattering states. Another "number" is the sign of energy which determines the wave function in the leads, namely, distinguishes between the u and the v spinors given in Eq. (11). The reflection symmetry defined in the previous section converts left movers into right movers:

$$Sv_{k,p}e^{ipy} = z_p v_{k,-p}e^{-ipy}, \quad Su_{k,p}e^{ipy} = -z_p u_{k,-p}e^{-ipy}, \tag{35}$$

where we suppressed the index k in $z_{kp} = (k + ip)/\varepsilon_{\mathbf{k}}$.

The "out-of-barrier" equation is just the free Weyl equation with negative and positive energy solutions, $\psi = u_{kp}e^{i(kx+py)}$ (hole) and $\psi = v_{kp}e^{i(kx+py)}$ (electron) discussed in the previous Section. It should be matched with the "in-barrier" solution. Several distinct kinematic possibilities exist. We survey them from high to low, see Fig. 3.

(1) This is the case with energies above the barrier, $\varepsilon > U$.Both inside and outside one has electron v states with different momenta. Outside the barrier $p = \sqrt{\varepsilon^2 - k^2}$, while inside the barrier, the momentum in the field direction is

$$q = \sqrt{(\varepsilon - U)^2 - k^2}. \tag{36}$$

One has a wave (real q) inside for

$$p > p_2 \equiv \sqrt{(U + 2|k|)\,U}. \tag{37}$$

The lower bound, $p_2(k)$, is the green line in Fig. 3. There is an evanescent (imaginary momentum q) particle state inside for

$$\sqrt{U^2 - k^2} \equiv p_U(k) < p < p_2. \tag{38}$$

Crossing the red line in Fig. 3, $p_U(k)$, one encounters states below the barrier.

(2) In this case, positive energy states are below the barrier, $0 < \varepsilon < U$. One has the v spinor (electron) outside the barrier, while the u spinor (hole) inside. For momenta p in the range

$$\sqrt{(U - 2|k|)\,U} \equiv p_1 < p < p_U, \tag{39}$$

the states are evanescent hole states. At yet lower energies, $p < p_1$, one has a propagating state, but this time is a hole. This relativistic feature is the cause of the Klein paradox.

(3) Next are negative energy states, $\varepsilon < 0$. Outside the barrier now one has $\varepsilon = -\sqrt{p^2 + k^2}$. This is another purely "relativistic" possibility in which one has holes both outside and hence inside the barrier. The Schrödinger equation above the barrier $\varepsilon > U$ is solved by the scattering states for right movers, $p > 0$,

$$\phi_{kp}(y) = \frac{1}{\sqrt{DW}} \begin{cases} v_{kp}e^{ipy} + r_{kp}v_{k,-p}e^{-ipy}, & \text{for} \quad y < -L/2, \\ A_{kp}v_{kq}e^{iqy} + B_{kp}v_{k,-q}e^{-iqy}, & \text{for} \quad -L/2 < y < L/2, \\ t_{kp}v_{kp}e^{ipy}, & \text{for} \quad L/2 < y, \end{cases} \tag{40}$$

Matching conditions,

$$\begin{aligned} v_p e^{-ipL/2} + r_p v_{-p} e^{ipL/2} &= A_p v_q e^{-iqL/2} + B_p v_{-q} e^{iqL/2}, \\ t_p v_p e^{ipL/2} &= A_p v_q e^{iqL/2} + B_p v_{-q} e^{-iqL/2}, \end{aligned} \tag{41}$$

(where the fixed index k is suppressed) determine the T matrix and are easily solved. The electron v states have to be replaced with u states in the case of a hole, so in the second energy region in the barrier part, $v \to u$, while in the third energy region in all parts, $v \to u$. For example, for evanescent modes below the barrier one obtains

$$t_{kp} = \frac{\left(z_p^2 - 1\right)\left(z_q^2 - 1\right)}{e^{-iqL}(1 - z_p z_q)^2 - e^{iqL}(z_p - z_q)^2}. \tag{42}$$

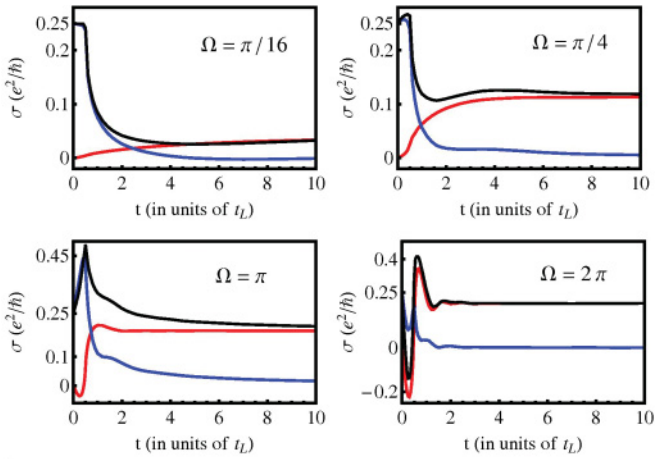

FIG. 4. (Color online) Conductivity of finite-length samples for $\Omega = UL/\hbar v_g = \pi/16, \pi/4, \pi, 2\pi$. Red line is the intraband contribution, blue line is the interband contribution, black line is the total conductivity. The time is given in units of $t_L = L/v_g$, while the unit of conductivity is $e^2/\hbar$.

C. LB conductance

According to the LB formula one has to sum up the transmission coefficients $T_{kp} = |t_{kp}|^2$ over all the states, namely, over the regions 1–3 that obey the constraint $p(k) = \sqrt{\mu^2 - k^2}$. The chemical potential $\mu = U + U_{\text{gate}}$ of graphene is counted here from the bottom of the barrier and let us consider only positive U_{gate}. In this case, region 3, in which energy is negative, and region 2, where energy is positive but not large enough, therefore will not contribute and we are left with region 1 of the previous section:

$$G = \frac{4e^2}{2\pi} \sum_{|k|<|\mu|} |t_{k,p(k)}|^2. \tag{43}$$

Let us first consider, following Ref. 15, only evanescent-states contributions under the barrier. Although finite sample width with various boundary conditions can be easily considered, we take a limit of infinite aspect ratio $W/L \to \infty$ and generally replace summation over $k \equiv k_x$ in Eq. (43) by an integral. In this case one can form two dimensionless combinations: the barrier "strength" $UL \equiv \Omega$ and $U_{\text{gate}}L$. It turns out (not shown in the present paper) that the conductance has a smooth limit $U_{\text{gate}}L \to 0$ that, of course, involves evanescent states only. One therefore can study directly the case of $U_{\text{gate}} = 0$. Substituting the transmission coefficient of Eq. (42), one obtains the following limiting value of conductivity:

$$\sigma_{LB}(\Omega) = G_{LB}\frac{L}{W} = \frac{2e^2LU^2}{\pi^2}\int_{k=0}^{U}\frac{U^2-k^2}{U^2\cosh^2(kL)-k^2} = \frac{2e^2\Omega}{\pi^2}\int_{\bar{k}=0}^{1}\frac{1-\bar{k}^2}{\cosh^2(\bar{k}\Omega)-\bar{k}^2}, \tag{44}$$

where the dimensionless momentum $\bar{k} = k/U$ is used. The result for various Ω appears in Fig. 4 as the long-time limit.

For large Ω, the integral is dominated by small $\bar{k}$ and one gets the "mesoscopic" value of conductivity,

$$\sigma_{LB}(\Omega) = \frac{2e^2\Omega}{\pi^2}\int_{\bar{k}=0}^{1}\cosh^{-2}(\bar{k}\Omega) = \frac{2e^2}{\pi^2} = \sigma_1. \tag{45}$$

One, therefore, can apply the dynamical approach to try to understand the crossover from the short ballistic time, the electron-hole "bulk" dynamics, to the long ballistic time, the barrier reflection dominated dynamics.

D. Electron tunneling into graphene from leads for $U = U_{\text{gate}}$

The main physical effect of leads is that they "contaminate" the graphene flake (assumed to be at Dirac point). Electrons from the lead metal tunnel into the flake creating charge "puddles" on both sides of the barrier. As a result the intraband channel for electric transport is greatly enhanced for small flakes and might dominate over the interband channel, especially at small fields. The quantitative consideration of this contamination is more transparent in the basis of symmetric and antisymmetric eigenfunctions than it would be in the scattering states basis (which was convenient for the LB approach above).

The symmetry image of the scattering state $\phi_{k,p}(r)$ defined in Eq. (40) is $\phi_{k,-p}(r) = \widehat{S}\phi_{k,p}(r)$, where the symmetry operator $\widehat{S}$ was defined in Eq. (32). Above the barrier (region 1), $\varepsilon > U$, one can write symmetric (s)/antisymmetric (a) functions as (with the x dependence of the wave functions e^{ikx} implied and index k suppressed):

$$\phi_p^{s,a}(y) = \frac{1}{\sqrt{2}}(1 \pm \widehat{S}), \quad \phi_p(y) = \frac{1}{\sqrt{2DW}}\begin{cases} \left(e^{ipy} + \sigma_x D_p^{s,a} e^{-ipy}\right) v_p, & \text{for } y < -L/2, \\ \pm(e^{iqy} + \sigma_x e^{-iqy}) E_p^{s,a} v_q, & \text{for } -L/2 < y < L/2, \\ \pm\left(D_p^{s} e^{ipy} + \sigma_x e^{-ipy}\right) v_p, & \text{for } L/2 < y, \end{cases} \tag{46}$$

where q is the momentum in the barrier range given in Eq. (36), and

$$D_p^{s,a} = \frac{r_p}{z_p} \pm t_p = e^{-ipL}\frac{z_pz_q - 1 \pm (z_p - z_q)e^{-iqL}}{z_p - z_q \pm (z_pz_q - 1)e^{-iqL}},$$
$$E_p^{s,a} = A_p \pm B_p z_{-q} = \frac{e^{-i(q+p)L/2}\left(z_p^2 - 1\right)}{z_p - z_q \pm (z_pz_q - 1)e^{-iqL}}. \tag{47}$$

Below the barrier for the positive energy states (region 2) one similarly has the same form

$$\phi_p^{s,a}(y) = \frac{1}{\sqrt{2DW}} \begin{cases} \left(e^{ipy} + \sigma_x D_p'^{s,a} e^{-ipy}\right) v_p, & \text{for } y < -L/2, \\ (\pm e^{iqy} + \sigma_x e^{-iqy}) E_p'^{s,a} u_q, & \text{for } -L/2 < y < L/2, \\ \pm\left(D_p'^{s,a} e^{ipy} + \sigma_x e^{-ipy}\right) v_p, & \text{for } L/2 < y, \end{cases} \tag{48}$$

with different coefficients

$$D_p'^{s,a} = -e^{-iLp} \frac{1 + z_p z_q \mp (z_p + z_q) e^{-iLq}}{z_q + z_q \mp (z_p z_q - 1) e^{-iLq}}, \quad E_p'^{s,a} = \frac{e^{-iL(p+q)/2}\left(z_p^2 - 1\right)}{z_q + z_q \mp (z_p z_q + 1) e^{-iLq}}. \tag{49}$$

The negative energy states (region 3) are obtained from those in region 1 by a replacement $v \to u$.

$$\varphi_p^{s,a}(y) = \frac{1}{\sqrt{2DW}} \begin{cases} \left(e^{ipy} + \sigma_x D_p^{s,a} e^{-ipy}\right) u_p, & \text{for } y < -L/2, \\ \pm\left(e^{iqy} + \sigma_x e^{-iqy}\right) E_p^{s,a} u_q, & \text{for } -L/2 < y < L/2, \\ \pm\left(D_p^{s} e^{ipy} + \sigma_x e^{-ipy}\right) u_p, & \text{for } L/2 < y. \end{cases} \tag{50}$$

We infer that physically the leads induce charge "puddles" in graphene at the Dirac point. These electrons can now be accelerated (in an ultrarelativistic fashion by reorientation) and compete with the electron-hole channel described above.

IV. CURRENT EVOLUTION IN GRAPHENE WITH BARRIER

A. The bias and the electric current in basis of the barrier eigenstates

Now we calculate the evolution of the current density within the linear response approximation. The dynamics of the many-body system with the contact potential barrier after switching on the electric field is determined in the Heisenberg picture by the equation

$$i\,\partial_t \hat{\psi}(t) = (K + V)\,\hat{\psi}(t), \tag{51}$$

where the K is defined in Eq. (30) and V in Eqs. (8) and (14).

The unperturbed part of the Hamiltonian, $\widehat{K}$, is diagonalized by choosing a basis linked to the eigenfunctions of the first quantized operator H_{1Q}, Eq. (34):

$$\hat{a}_{kp}^S = \int_r \phi_{kp}^{S\dagger}(r)\hat{\psi}_r, \quad \hat{b}_{kp}^S = \int_r \varphi_{kp}^{S\dagger}(r)\hat{\psi}_r, \\ \hat{\psi}_r = \sum_{kpS} \left[\phi_{kp}^S(r)\hat{a}_{kp}^S + \varphi_{kp}^S(r)\hat{b}_{kp}^S\right], \tag{52}$$

so that $\hat{K} = \sum_\lambda \varepsilon_{kp}(\hat{a}_\lambda^\dagger \hat{a}_\lambda - \hat{b}_\lambda^\dagger \hat{b}_\lambda)$, where λ combines k, p, and S. The operator $\hat{a}^\dagger$ ($\hat{b}$) creates an electron (hole), and summations are over symmetric and antisymmetric states, $S = a,s$ with $p > 0$. The perturbation operator in the new basis takes the form

$$\hat{V} = \sum_{\lambda,\sigma} (V_{\lambda\sigma}^{++}\hat{a}_\lambda^\dagger \hat{a}_\sigma + V_{\lambda\sigma}^{-+}\hat{b}_\lambda^\dagger \hat{a}_\sigma + V_{\lambda\sigma}^{+-}\hat{a}_\lambda^\dagger \hat{b}_\sigma + V_{\lambda\sigma}^{--}\hat{b}_\lambda^\dagger \hat{b}_\sigma). \tag{53}$$

For example, the electron-hole matrix element is given by

$$V_{kl;k'p}^{-+ST} = \int_{xy} e^{i(k'-k)x} V(y) \varphi_{kl}^{S\dagger}(y) \phi_{k'p}^{T}(y) \\ = W\delta_{kk'} \mathcal{V}_{k,lp}^{-+ST}, \tag{54}$$

where

$$\mathcal{V}_{k,lp}^{-+ST} = \int_y V(y) \varphi_{kl}^{S\dagger}(y) \phi_{kp}^{T}(y). \tag{55}$$

In the middle of the sample, the current operator is

$$\hat{I}_y(y=0) = \int_x \hat{j}_y(x,0) = \sum_{\lambda,\sigma} (j_{\lambda\sigma}^{++}\hat{a}_\lambda^\dagger \hat{a}_\sigma + j_{\lambda\sigma}^{-+}\hat{b}_\lambda^\dagger \hat{a}_\sigma \\ + j_{\lambda\sigma}^{+-}\hat{a}_\lambda^\dagger \hat{b}_\sigma + j_{\lambda\sigma}^{--}\hat{b}_\lambda^\dagger \hat{b}_\sigma), \tag{56}$$

where, for example,

$$j_{k'p;kl}^{+-TS} = W\delta_{kk'} j_{k,pl}^{+-TS}; \quad j_{k,pl}^{+-TS} = -4e\phi_{kp}^{T\dagger}(0)\sigma_y \varphi_{kl}^{S}(0). \tag{57}$$

The factor four appears due to spin degeneracy and two Dirac points (valley degeneracy). Now one can write the first-order contributions to the electric current induced by the perturbation.

B. General expressions for the interband and the intraband contributions to current in linear response

In linear response, one obtains at gate potential U_{gate} (assumed positive) two contributions with completely different physical interpretations. In the first term, the summation is over electron states above $\mu = U + U_{\text{gate}}$ and electron states below the Fermi level,

$$I_{ee}(t) = -W \sum_k \sum_{p:\varepsilon_{kp}>\mu} \sum_{l:\varepsilon_{kl}<\mu} \frac{1 - e^{-i(\varepsilon_{kp}-\varepsilon_{kl})t}}{\varepsilon_{kp} - \varepsilon_{kl}} \\ \times \mathcal{V}_{k,lp}^{++ST} j_{k,pl}^{++TS} + \text{c.c.} \tag{58}$$

The summation over symmetry indices T and S is understood. The second contribution sums over electrons above μ and all the hole states with arbitrary l:

$$I_{eh}(t) = -W \sum_{k,l} \sum_{p:\varepsilon_{kp}>\mu} \frac{1 - e^{-i(\varepsilon_{kp}+\varepsilon_{kl})t}}{\varepsilon_{kp} + \varepsilon_{kl}} \\ \times \mathcal{V}_{k,lp}^{-+ST} j_{k,pl}^{+-TS} + \text{c.c.} \tag{59}$$

The hole's momentum has no restriction since its energy is always negative, while $U_{\rm gate}$ is positive (in this work we do not consider the case $U_{\rm gate} < 0$, that was discussed recently in Ref. 31 in the framework of LB approach, where other possibilities can occur). The first contribution is the "one-particle" type (the intraband channel), very much like in more common many-body electronic systems. The second contribution, to the contrary, is purely ultrarelativistic (the interband channel) and describes the electron-hole pair creation, very much like in the infinitely long flake discussed in Sec. II.

It is useful to define an effective dimensionless conductivity. There are only two time scales in the problem: the inverse barrier height $t_U = 1/U$ ($\hbar/U$ in physical units) and the flight time to cross the sample $t_L = L$ (L/v_g) with the ratio being the only "material" parameter $\Omega = UL = t_L/t_U$ in the linear response considerations. For this case, the effective conductivity has a scaling property:

$$\sigma\,(U,L,t) = \frac{I\,(U,L,t)}{V_0}\frac{L}{W} = \sigma(\Omega,\bar{t}). \tag{60}$$

The scaled time is defined, as in Sec. II, $\bar{t} = t/t_L$. Since in the dynamical approach the limit $U_{\rm gate} \to 0$ is smooth,[17] in what follows the conductivity will be calculated directly for $U_{\rm gate} = 0$. We concentrate on the case when quantizations of k_x and k_y are not important (the generalization to the discrete case is straightforward), the sums in Eqs. (58) and (59) can be replaced by integrals over the dimensionless momentum variables $k = U\bar{k}$, $p = U\bar{p}$, and $\bar{p}_U = \sqrt{1-\bar{k}^2}$. The intraband contribution becomes

$$\sigma^{ee}(\bar{t}) = -2\frac{LU^2}{V_0}\frac{W}{2\pi}\left(\frac{D}{2\pi}\right)^2\int_{\bar{k}=0}^{1}\int_{\bar{l}=0}^{\bar{p}_U}\int_{\bar{p}=\bar{p}_U}^{\infty} \times\frac{1-e^{-i(\epsilon-\epsilon')\Omega\bar{t}}}{\epsilon-\epsilon'}\mathcal{V}_{lp}^{++ST}\,j_{pl}^{++TS} + \text{c.c.} \tag{61}$$

Here, rescaled energies, $\epsilon \equiv \varepsilon_{kp}/U$, $\epsilon' \equiv \varepsilon_{kl}/U$ in addition to momentum, $\bar{k}$, $\bar{p}$, and $\bar{l}$ are used and the factor two comes from positive and negative k. Similarly, the interband contribution to conductivity takes the form

$$\sigma^{eh}(\bar{t}) = -2\frac{LU^2}{V_0}\frac{W}{2\pi}\left(\frac{D}{2\pi}\right)^2\int_{\bar{k}=0}^{1}\int_{\bar{l}=0}^{\infty}\int_{\bar{p}=\bar{p}_U}^{\infty} \times\frac{1-e^{-i(\epsilon+\epsilon')\Omega\bar{t}}}{\epsilon+\epsilon'}\mathcal{V}_{lp}^{-+ST}\,j_{pl}^{+-TS} + \text{c.c.} \tag{62}$$

Next, we consider the two contributions in turn.

V. THE INTRABAND CONTRIBUTION

A. The electron-electron matrix elements in linear response

Neglecting the dependencies on the cutoff and keeping notations used in Sec. IV A, one obtains, after some algebra, the following expressions for the matrix elements for the electron-electron contribution for $T \neq S$,

$$\mathcal{V}_{lp}^{++TS} = \frac{ieV_0}{2DW}\Big\{(1+z_l^* z_p)\frac{D_l'^{T*}D_p^S e^{i(p-l)L/2} - e^{-i(p-l)L/2}}{p-l} + (z_p+z_l^*)\frac{D_p^S e^{i(p+l)L/2} - D_l'^{T*}e^{-i(p+l)L/2}}{p+l} - 4E_l'^{T*}E_p^S[(1-z_q z_g^*)f(g-q) + (z_q - z_g^*)f(g+q)]\Big\}. \tag{63}$$

where the function f is defined as

$$f(q) = \frac{\sin(qL/2)}{q^2} - \frac{L}{2}\frac{\cos(qL/2)}{q}. \tag{64}$$

It is important to note that the dominant contributions to the integrals in Eq. (61) come from the $(p-l)^{-1}$ poles. The corresponding current density matrix elements are

$$\begin{aligned} j_{pl}^{++sa} &= i\frac{e}{WD}E_p^{s*}E_l'^{a}(1+z_q^*)(1+z_g),\\ j_{pl}^{++as} &= -i\frac{e}{WD}E_p^{a*}E_l'^{s}(1-z_q^*)(1-z_g). \end{aligned} \tag{65}$$

The one-particle (electron-electron) contribution to the scaled conductivity, Eq. (60), is shown in Fig. 4 as red curves for various values of Ω as function of time $\bar{t}$. At times shorter than both t_L and t_U, it rises linearly. For $\Omega > 1$, the conductivity oscillates before eventually approaching the LB result of Sec. III C. In the following sections, the two ballistic regimes, namely, the limit of long times $t \gg t_U, t_L$ (or in scaled form $\bar{t} \gg 1/\Omega, 1$) and short times $t \ll t_U, t_L$ (or in scaled form $\bar{t} \ll 1/\Omega, 1$) are analyzed analytically.

B. Short time asymptotics

Expanding the electron-electron contribution to the conductivity, Eq. (61), to leading order in the short-time limit yields

$$\sigma^{ee} = -i\bar{t}\frac{e^2\Omega}{\pi^3}\int_{\bar{k}=0}^{1}\int_{\bar{l}=0}^{\bar{p}_U}\int_{\bar{p}=\bar{p}_U}^{\infty}\mathcal{V}_{lp}^{++ST}\,j_{pl}^{++TS} + \text{c.c.} \tag{66}$$

This leads to a small conductivity contribution since the integration range on the variable $\bar{l}$ is rather limited. The linear behavior of the conductivity is shown in Fig. 4 (red lines). For the case $\Omega \lesssim 1$ ($t_L < t_U$), represented in Fig. 4 by $\Omega = \pi/16, \pi/4$, the intraband contribution is positive and increases monotonically. However, when $\Omega > 1$ ($t_L > t_U$) represented in Fig. 4 by $\Omega = \pi, 2\pi$ it becomes negative.

C. Long-time asymptotics

Due to the oscillating functions in Eq. (61) the long-time asymptotics is due solely to the region of the three-dimensional integral when $\varepsilon_{kp} - \varepsilon_{kl} \to 0$. Consequently, in view of the discussion of the various kinematical regions in Sec. III B, summarized in Fig. 3, the limit is dominated by integrating over the transitions from evanescent states above the barrier (region 1) to evanescent states below the barrier (region 2). Since the integral is dominated by the neighbourhood of the line $\varepsilon_{kp},\varepsilon_{kl} \approx U$, one can expand around this line (the red line in Fig. 3), $\overline{p} \approx \overline{p}_U + \Delta p$, so that the evanescent momentum (in the field direction) is, to second order, $\overline{k} - \frac{\overline{p}_U^2}{2\overline{k}}\Delta p^2$. Similar expansions are made for the momentum $\overline{l}$. Therefore one can simplify the expression for the conductivity by replacing the integrand in Eq. (61)) by its limiting value. Albeit, this limit is nontrivial. In particular, the lower components of the spinor in Eq. (11) is just

$$z_p \to Z \equiv \overline{k} + i\overline{p}_U, \quad z_q = \frac{\overline{p}_U}{2\overline{k}}\Delta p. \tag{67}$$

As a result the coefficients determining the eigenstates, Eqs. (47) and (49), simplify considerably:

$$\begin{aligned} E_p^{a,s} = E_l'^{a,s} &\to e^{\Omega(\overline{k}-i\overline{p}_U)/2}\frac{Z^2-1}{Z \pm e^{\Omega\overline{k}}}, \\ D_p^{a,s} = D_l'^{a,s} &\to -e^{-i\Omega\overline{p}_U}\frac{1+Ze^{\Omega\overline{k}}}{Z \pm e^{\Omega\overline{k}}}. \end{aligned} \tag{68}$$

Since at small κ, $f(\kappa) \simeq \frac{L^3}{24}\kappa$, the third contribution to the perturbation matrix elements, Eq. (63), is negligible. The results for the matrix elements of the perturbation and the current are

$$\begin{aligned} \mathcal{V}_{lp}^{as} = -\mathcal{V}_{lp}^{sa*} &= \frac{2eVU}{DW}\frac{\overline{p}_U}{i\overline{p}_U - \sinh(\Omega\overline{k})}\frac{1}{\overline{p}-\overline{l}}, \\ j_{pl}^{sa} = j_{pl}^{as*} &= -\frac{8ie}{DW}\frac{\overline{p}_U^2}{i\overline{p}_U + \sinh(\Omega\overline{k})}. \end{aligned} \tag{69}$$

Substituting these matrix elements into Eq. (61), one obtains the contribution to the conductivity:

$$\begin{aligned} \sigma^{ee}(\overline{t}) = \frac{16e^2\Omega}{\pi^3}\int_{\overline{k}=0}^{1}\frac{\overline{p}_U^3(\overline{k})}{\cosh^2(\Omega\overline{k})-\overline{k}^2} \\ \times \int_{\overline{l}=0}^{\overline{p}_U}\int_{\overline{p}=\overline{p}_U}^{\infty}\frac{\sin[(\epsilon-\epsilon')\Omega\overline{t}]}{\epsilon-\epsilon}\frac{1}{\overline{p}-\overline{l}}, \end{aligned} \tag{70}$$

Since $\overline{p}-\overline{l} \approx (\epsilon-\epsilon')/\overline{p}_U$, one gets for the last two integrals:

$$\begin{aligned} &\overline{p}_U(k)\int_{\epsilon'=\overline{k}}^{1}\int_{\epsilon=1}^{\infty}\frac{\epsilon\epsilon'}{\sqrt{\epsilon^2-\overline{k}^2}\sqrt{\epsilon'^2-\overline{k}^2}}\frac{\sin[(\epsilon-\epsilon')\Omega\overline{t}]}{(\epsilon-\epsilon')^2} \\ &\quad\approx \frac{1}{\overline{p}_U(k)}s(\overline{k},\Omega\overline{t}), \end{aligned} \tag{71}$$

where the function

$$s(\overline{k},\tau) = \int_{\epsilon'=\overline{k}}^{1}\int_{\epsilon=1}^{\infty}\frac{\sin[(\epsilon-\epsilon')\tau]}{(\epsilon-\epsilon')^2} \to_{\tau\to\infty} \frac{\pi}{2}. \tag{72}$$

Therefore at large times $t > t_U$, one finally obtains

$$\sigma^{ee}(\Omega) = \frac{2e^2\Omega}{\pi^2}\int_{\overline{k}=0}^{1}\frac{1-\overline{k}^2}{\cosh^2(\Omega\overline{k})-\overline{k}^2} = \sigma_{LB}(\Omega). \tag{73}$$

This is one of the main results of the paper. The electron-electron contribution converges to the LB result, Eq. (44), at large times. Furthermore, with large Ω the conductivity is dominated by infinitesimal $\overline{k}$ and consequently can be written as

$$\sigma^{ee} = \frac{e^2\Omega}{\pi^3}\frac{\pi}{2}\int_{\overline{k}=0}^{1}\frac{1}{\cosh^2(\overline{k}\Omega)} = \frac{e^2}{2\pi}\frac{1}{\pi}. \tag{74}$$

Thus, for four flavours, we reproduce σ_1, Eq. (2), starting from the dynamical approach.

VI. THE INTERBAND CONTRIBUTION

A. The electron-hole matrix elements in linear response

Similarly to the above, the matrix elements for the electron-hole Landau-Zener-Schwinger contribution read (with $T \neq S$):

$$\begin{aligned} \mathcal{V}_{lp}^{-+TS} = \frac{ieV}{2DW}\Big\{ &\left(z_p - z_l^{-1}\right)\frac{D_p^S e^{i(p+l)L/2} + D_l^{*S}e^{-i(p+l)L/2}}{p+l} \\ &- \left(1 - z_p z_l^{-1}\right)\frac{D_l^{*S}D_p^S e^{i(p-l)L/2} + e^{-i(p-l)L/2}}{p-l} \\ &+ 4E_l^{S*}E_p^S\big[\left(1-z_q z_g^{-1}\right)f(g-q) \\ &+ \left(z_q - z_g^{-1}\right)f(g+q)\big]\Big\}. \end{aligned} \tag{75}$$

Unlike the intraband contribution of the previous section, the p-l pole is cancelled by a numerator (both p and l are positive) and therefore the contribution will not be dominated by the evanescent states. The correspondent current density matrix elements are

$$\begin{aligned} j_{pl}^{+-sa} &= -\frac{ie}{WD}E_p^{s*}E_l^s\left(1+z_q^{-1}\right)(1+z_g), \\ j_{pl}^{+-as} &= \frac{ie}{WD}E_p^{a*}E_g^a\left(1-z_q^{-1}\right). \end{aligned} \tag{76}$$

The expression for conductivity $\sigma^{eh}(U,L,t)$ is UV divergent like the conductivity of the infinite sample $\sigma(U=0,L,t) \equiv \sigma_0(\overline{t})$ biased in the region of length L that was studied in Sec. II. B (and which is solely due to the electron-hole pairs). The difference $\Delta\sigma^{eh}(\overline{t}) = \sigma^{eh}(U,L,t) - \sigma_0(\overline{t})$ however is finite. Using Eq. (62) for σ^{eh}, the difference can be written as an integral over a limited domain of momenta in the field direction:

$$\begin{aligned} \Delta\sigma^{eh}(\overline{t}) = -\frac{\Omega U(WD)^2}{4\pi^3 V_0}\int_{\overline{l}=0}^{\infty}\int_{\overline{k}=0}^{1}\int_{\overline{p}=0}^{\overline{p}_U} \\ \times \frac{1-e^{-i(\epsilon+\epsilon')\Omega\overline{t}}}{\epsilon+\epsilon'}\mathcal{V}_{lp}^{++ST}j_{pl}^{++TS} + \text{c.c.} \end{aligned} \tag{77}$$

The results, for $U_{\text{gate}} = 0$, are given in Fig. 4 for several Ω as blue lines and were discussed in Sec. II. At small times it starts with the ultrarelativistic value $\sigma_2 = 1/4$ and at relatively large times ($t_U \gg t > t_L$) it decays as $1/4\pi\overline{t}$. This short-time value σ_2 does not change when $U > 0$ provided

the time is smaller than $t_L/2$. This follows from the fact that in relativistic graphene, information about the barrier cannot arrive at the center of the sample before that time. The long-time asymptotics in the presence of the barrier is considered next.

B. Long-time asymptotics

Due to oscillations, the long-time behavior of the electron-hole contribution is dominated by the region $\varepsilon_{kp} + \varepsilon_{kl} \to 0$ in the integrations in Eq. (77). Unlike for the intraband contribution in the last Section, in this case all three momenta k, p, and l in Eq. (77) are small. In this limit, $q, g \to 1$, and hence the phases $z_q, z_g \to i$ and the function $f(g+q) \to -\frac{1}{4}[\Omega\cos(\Omega) - \sin(\Omega)]$ and $f(g-q) \to 0$. Therefore it is simple to calculate $\Delta\sigma^{eh}$ for special values of Ω. This is done in the Appendix. Numerical results show that $\Delta\sigma^{eh}(\Omega = 3\pi/2 + 2\pi N)$, $\Delta\sigma^{eh}(\pi/2 + 2\pi N) \propto 1/\bar{t}^3$, while $\Delta\sigma^{eh}(\pi + 2\pi N) = -\Delta\sigma^{eh}(2\pi N) \approx 1/4\pi\bar{t}$. One can fit the long-time asymptotics as $\Delta\sigma^{eh} \sim \cos(\Omega)/4\pi\bar{t}$.

VII. DISCUSSION AND CONCLUSIONS

Two different kinds of ballistic behavior occur in undoped graphene (graphene at Dirac point) at zero temperature. The first one is a very unusual "ultrarelativistic" interband physics. Electron-hole pairs are copiously created via Landau-Zener-Schwinger's mechanism by an applied electric field. It is independent on leads and finite-size effects of the graphene sample. On the contrary, the intraband physics in the second kind is highly sensitive to finite-size effects and contact potentials. The interband transition results, within linear response, in the universal bulk value σ_2 of conductivity, while the intraband transition is characterized by a shape-dependent linear response with the effective conductivity σ_1 for large aspect ratio rectangular flakes.

Now we recapitulate under what conditions either of these two processes is dominant in experiments on a time scale $1/\omega$ in an ac electric field E (or in a pulse of duration $1/\omega$) for a graphene flake of length L (in the limit of large width W, although the discussion can be easily extended to finite aspect ratios) and a contact barrier potential U. Here, we classify various practically important ranges of sample (U, L) and experimental (ω, E) parameters. We note that our analysis, based on the effective low-energy Weyl Hamiltonian (34), is valid even for the large fields $E \sim 10^6$ V/m studied recently,[30] which are yet smaller than $\gamma/ae \sim 10^{10}$ V/m.

A. "Unintrusive" experiments, $U = 0$

In reflectance and transmission experiments in visible to mid IR or even microwave range,[39] there are no leads, hence no potential barrier, $U = 0$. The interband (Landau-Zener-Schwinger) process is dominant for any practical length and electric field E. However, the transport can be either linear or highly nonlinear.

(i) For $1/\omega < t_{\rm nl} = \sqrt{\hbar/eEv_g}$ one has linear response, $J = \sigma_2 E$, with the interband value of conductivity $\sigma_2 = \frac{\pi}{2}\frac{e^2}{h}$. In this case the nonlinear Schwinger's pair creation regime is not yet reached. The conductivity is real and frequency independent (no inductive part). There are small frequency-dependent corrections to linear response [the E^3 correction to both real and imaginary part and third harmonic generation was calculated in Ref. 27, see Eqs. (53) and (54) therein].

(ii) For $1/\omega > t_{\rm nl}$ *and* $t_{\rm nl} < t_L = L/v_g$, the transport is still dominated by electron-hole channel, but is nonlinear. The electron-hole pairs are efficiently created due to the LZS mechanism with rate proportional to $E^{3/2}$. This results in following the I-V curve, see Eq. (27):

$$J = \frac{eL}{\pi^2}\left(\frac{eE}{\hbar}\right)^{3/2}. \tag{78}$$

(iii) For $1/\omega > t_{\rm nl}$ *and* $t_{\rm nl} > t_L$, the transport is still dominated by electron-hole channel and the LZS process, but since the electric field is applied in the limited space (length L which is not large enough) and the current is much smaller, see Eq. (28),

$$J = \frac{2eL^2}{\pi^2 v_g}\left(\frac{eE}{\hbar}\right)^2. \tag{79}$$

B. Large barrier

In samples on substrate with metallic leads, the work functions of the graphene and the metal are typically different and as a result the contact potential difference is of order $U = 0.1$–1 eV, see calculations in Ref. 13 and references therein. It can be both positive and negative. In this case, the corresponding time scale $t_U = \hbar/U < 7$ fs, which is typically smaller than any of the other scales $t_L = L/v_g$, $t_{\rm nl} = \sqrt{\hbar/eEv_g}$. This leads to an effective suppression of the electron-hole channel for all the frequencies in the infrared range and smaller (including dc) and the physics is dominated by the electron-electron channel.

(i) $1/\omega > t_U$. The dc conductance is given by the Landauer-Bütticker formula, generalized in Eq. (44), and is more sensitive to the properties of the leads than those of graphene. When graphene is "nominally" at the Dirac point, namely, when the chemical potential of the lead is on the barrier, graphene is still contaminated by charges tunneling into the stripe from the leads. These electrons are accelerated and lead to the mesoscopic type of conductance. For a large aspect ratio, the effective conductivity is $\sigma_1 = \frac{4}{\pi}\frac{e^2}{h}$. The assumption of an "infinite" barrier was made early on in Ref. 15 in order to develop the mesoscopic approach to transport in graphene. Surprisingly, this assumption still returns σ_1 even though $U \gg \gamma \approx 2.7$ eV and intervalley interactions could be important.

(ii) $1/\omega < t_U$. The high-frequency (microwave and above) experiments are done without leads. However, if one had a setup with leads, it could not significantly alter the pseudo-Ohmic behavior with $\sigma = \sigma_2$ since the contaminated regions constitute only a small fraction of the sample. There is no effect of ballistic acceleration across the sample for large frequencies or short pulses.

C. Small barrier

For certain materials and geometries, the potential barrier may be much smaller, of the order 0.01 eV (for example the

Ti lead in the $\beta = \pi/2$ geometry has -0.04 eV, while Ni in geometry $\beta = \pi$ has 0.04 eV, see Ref. 13 for details). It is feasible that the barrier even can be tuned to zero. It is not clear what is the contact barrier in the suspended graphene systems. It is reasonable to assume that for suspended samples the barrier is smaller due weaker coupling. Moreover, even in two-probe experiments on suspended graphene, the Dirac point appeared exactly at zero bias voltage[2,3] (compared to up to 40 V in sampled on substrate) and there are less charge "puddles." That also signals that the leads do not create the puddles. In such a case a variety of crossover phenomena might occur when t_U is comparable to $t_{\rm nl}$ or t_L studied here.

D. Finite-size and topology effects

The calculations made in the present paper can be easily generalized to a finite or even small flake width W (assumed infinite here). In fact, it was shown numerically,[33] that in graphene nanoribbons modeled by a tight-binding model, one observes a crossover from σ_2 to $\sigma_{1\rm ribbon} = e^2/h$ at a time roughly corresponding to t_L. The value of $\sigma_{1\rm ribbon}$ in this model is different from $\frac{4}{\pi}\frac{e^2}{h}$ due to the different topology and was calculated in Ref. 40. In Fig. 3 of Ref. 33, the time evolution of current for $t = 0{-}10^3 t_L$ is shown. The current rises from zero and settles on σ_2 (via oscillations) on the microscopic time scale of $t_\gamma = \hbar/\gamma \approx 2.6 \times 10^{-16}$ s. This time scale is not seen in the Weyl model (it appears as an ultraviolet cutoff). Yet similar results, including oscillations, were obtained in the solution of the tight-binding model of the infinite sample.[17] The crossover from the initial interband to the intraband behavior also occurs as a series of oscillations around the value $\sigma_{1\rm ribbon}$. The period of oscillations in Fig. 3 in Ref. 33 is roughly t_L, as it is also the case in our Fig. 4 for large Ω. It is not easy to compare these results directly, since the microscopic model for leads cannot be readily translated into a potential barrier U of the continuum model. However, the similarity with our results suggests that $\Omega = UL/\hbar v_g \gg 1$, since their number of oscillations is large.

Our calculation is trivially extended to any system with Dirac point-like spectrum, like double layer graphene and the recently synthesized family of materials called "topological insulators"[41] in which surface excitations are similar to those in graphene with notable exception of the chirality. Schwinger's mechanism is also expected in these materials since chirality was not involved (left and right movers contributed equally to the emission rate of graphene). On the contrary, the effects of the sample topology probably require applications of sophisticated methods like the conformal mapping used in Ref. 32.

Finally, let us remark on the role of the Klein paradox in ballistic transport in graphene. While the pair creating mechanism can be linked to the Klein paradox behavior, the intraband mechanism at Dirac point does not make use of the states undergoing the Klein paradox. The Klein tunneling states described in Sec. III B 2 are characterized by energies in the range $0 < \varepsilon < U$, the states below the blue line in Fig. 3. These states make a contribution to the current at finite times, however, their contribution to the current at large times vanishes.

ACKNOWLEDGMENTS

We are indebted to K. H. Wu, E. Farber, W. B. Jian, V. Nazarov, H. C. Kao, Y. Lin, and S. Li for valuable discussions. Work of B. R. and D. N. was supported by NSC of Republic of China Grant No. 98-2112-M-009-014-MY3, the National Center for Theoretical Sciences, and MOE ATU program. M.L. acknowledges the hospitality and support of the NCTU, Electrophysics Department and MOE ATU program.

APPENDIX: LONG-TIME ASYMPTOTICS OF THE INTERBAND CONTRIBUTION FOR INTEGER VALUES OF $\Omega/(2\pi)$

In the long-time limit of the electron-hole conductivity, Eq. (77), the "under-the-barrier" momenta have a simple limit: $q, g \to 1$, so that the phases $z_q, z_g \to i$ and the function $f(g+q) \to -\frac{1}{4}[\Omega\cos(\Omega) - \sin(\Omega)]$ and $f(g-q) \to 0$.

When $\Omega = 2n\pi$, the wave function coefficients in Eq. (47) reduce to

$$\begin{aligned} E^s_p &= \frac{(-1)^n(1-i)}{2}(z_p+1), \\ E^a_p &= \frac{(-1)^n(1+i)}{2}(z_p-1), \\ D^s_p &= -D^a_p = 1. \end{aligned} \tag{A1}$$

Similarly, for $\Omega = (2n+1)\pi$, the wave-function coefficients in Eq. (47) become

$$\begin{aligned} E^s_p &= \frac{(-1)^n(1-i)}{2}(z_p-1), \\ E^a_p &= -\frac{(-1)^n(1+i)}{2}(z_p+1), \\ D^a_p &= -D^s_p = 1. \end{aligned} \tag{A2}$$

Thus the difference in conductivity due to barrier, Eq. (77), when Ω is even or odd integer of π, will clearly depend on n as (see notations in text)

$$\begin{aligned} \Delta\sigma^{eh}(\Omega) = \mp\frac{2\Omega e^2}{\pi^3}\int_{\bar l=0}^{\infty}\int_{\bar k=0}^{1}\int_{\bar p=0}^{\bar p_U}\frac{\sin[(\epsilon+\epsilon')\Omega\bar t]}{\epsilon+\epsilon'} \\ \times\left[\frac{1}{\bar p+\bar l}\left(\frac{\bar p}{\epsilon}+\frac{\bar l}{\epsilon'}\right)+\frac{1}{\bar p-\bar l}\left(\frac{\bar p}{\epsilon}-\frac{\bar l}{\epsilon'}\right)\right. \\ \left.-1-\frac{\bar k^2}{\epsilon\epsilon'}\right], \end{aligned} \tag{A3}$$

where "$-$" and "$+$" are corresponding to even and odd integer of $\Omega/2\pi$, respectively. Numerical results show that $\Delta\sigma^{eh}(\Omega = 2n\pi) \approx -\Delta\sigma^{eh}[\Omega = (2n+1)\pi] \approx 1/4\pi\bar t$.

When $\Omega = (2n \pm 1/2)\pi$, the wave-function coefficients in Eq. (47) can be rewritten as

$$\begin{aligned} E^s_p &= \frac{(-1)^n e^{-i\pi/4}}{2} z_p^{-1}\left(z_p^2-1\right), \\ E^a_p &= \frac{i(-1)^n e^{-i\pi/4}}{2}\left(z_p^2-1\right), \\ D^s_p &= -z_p^{-1}, \quad D^a_p = -z_p, \end{aligned} \tag{A4}$$

and

$$E_p^s = \frac{i\,(-1)^n\,e^{i\pi/4}}{2}\left(z_p^2-1\right),$$
$$E_p^a = \frac{(-1)^n\,e^{i\pi/4}}{2} z_p^{-1}\left(z_p^2-1\right), \qquad \text{(A5)}$$
$$D_p^s \to -z_p, \quad D_p^a = -z_p^{-1},$$

respectively. Hence one of the products of matrix elements vanishes: $\mathcal{V}_{lp}^{-+as}\, j_{pl}^{+-sa} + \mathcal{V}_{lp}^{-+sa}\, j_{pl}^{+-as} = 0$. That renders the difference of conductivity independent of Ω :

$$\Delta\sigma^{eh} = \mp 2\frac{e^2}{\pi^3}\int_{\bar{l}=0}^{\infty}\int_{\bar{k}=0}^{1}\int_{\bar{p}=0}^{\bar{p}_U}\frac{\sin[(\epsilon+\epsilon')\Omega\bar{t}]}{\epsilon+\epsilon'}\frac{\bar{p}^2\bar{l}^2}{\epsilon^2\epsilon'^2} \sim \bar{t}^{-3}. \qquad \text{(A6)}$$

*vortexbar@yahoo.com

[1] S. V. Morozov, K. S. Novoselov, M. I. Katsnelson, F. Schedin, D. C. Elias, J. A. Jaszczak, and A. K. Geim, Phys. Rev. Lett. **100**, 016602 (2008).

[2] X. Du, I. Skachko, A. Barker, and E. Y. Andrei, Nat. Nanotechnology **3**, 491 (2008).

[3] K. I. Bolotin, K. J. Sikes, J. Hone, H. L. Stormer, and P. Kim, Phys. Rev. Lett. **101**, 096802 (2008).

[4] E. A. Andrei, talk delivered at Workshop on Nonequilibrium Phenomena, Kanpur, 2010 (unpublished).

[5] K. S. Novoselov, A. K. Geim, S. V. Morozov, D. Jiang, M. I. Katsnelson, I. V. Grigorieva1, S. V. Dubonos, and A. A. Firsov, Nature (London) **438**, 197 (2005); Y. Zhang, Y. W. Tan, H. L. Stormer, and P. Kim, *ibid.* **438**, 201 (2005).

[6] A. H. Castro Neto, F. Guinea, N. M. R. Peres, K. S. Novoselov, and A. K. Geim, Rev. Mod. Phys. **81**, 109 (2009); N. M. R. Peres, *ibid.* **82**, 2673 (2010).

[7] E. Fradkin, Phys. Rev. B **33**, 3263 (1986); A. W. W. Ludwig, M. P. A. Fisher, R. Shankar, and G. Grinstein, *ibid.* **50**, 7526 (1994); V. P. Gusynin and S. G. Sharapov, *ibid.* **73**, 245411 (2006); S. Ryu, C. Mudry, A. Furusaki, and A. W. W. Ludwig, *ibid.* **75**, 205344 (2007); J. Cserti, *ibid.* **75**, 033405 (2007).

[8] It was noted by Ziegler in K. Ziegler, Phys. Rev. Lett. **97**, 266802 (2006); Phys. Rev. B **75**, 233407 (2007), different regularizations within the Kubo formalism resulted in different values of the dc conductivity.

[9] F. Xia, V. Perebeinos, Y. Lin, Y. Wu, and P. Avouris, Nat. Nanotechnology **6**, 179 (2011); X. Du, I. Skachko, A. Barker, and E. Y. Andrei, *ibid.* **3**, 491 (2008).

[10] V. N. Do and P. Dollfus, J. Appl. Phys. **106**, 023719 (2009); J. Phys. Cond. Mat. **22**, 425301 (2010).

[11] H. Schomerus, Phys. Rev. B **76**, 045433 (2007); J. P. Robinson and H. Schomerus, *ibid.* **76**, 115430 (2007); Y. M. Blanter and I. Martin, *ibid.* **76**, 155433 (2007).

[12] R. Golizadeh-Mojarad and S. Datta, Phys. Rev. B **79**, 085410 (2009).

[13] P. A. Khomyakov, A. A. Starikov, G. Brocks, and P. J. Kelly, Phys. Rev. B **82**, 115437 (2010).

[14] R. Danneau, F. Wu, M. F. Craciun, S. Russo, M. Y. Tomi, J. Salmilehto, A. F. Morpurgo, and P. J. Hakonen, Phys. Rev. Lett. **100**, 196802 (2008).

[15] J. Tworzydło, B. Trauzettel, M. Titov, A. Rycerz, and C. W. J. Beenakker, Phys. Rev. Lett. **96**, 246802 (2006).

[16] M. I. Katsnelson, Eur. Phys. J. B **51**, 157 (2006).

[17] M. Lewkowicz and B. Rosenstein, Phys. Rev. Lett. **102**, 106802 (2009).

[18] T. Ando, Y. Cheng, and H. Suzuura, J. Phys. Soc. Jap. **71**, 1318 (2002); N. M. R. Peres, F. Guinea, and A. H. Castro Neto, Phys. Rev. B **73**, 125411 (2006).

[19] L. A. Falkovsky and A. A. Varlamov, Eur. Phys. J. B **56**, 281 (2007).

[20] V. P. Gusynin, S. G. Sharapov, and J. P. Carbotte, Phys. Rev. Lett. **98**, 157402 (2007); H. Min and A. H. MacDonald, *ibid.* **103**, 067402 (2009).

[21] C. G. Beneventano, P. Giacconi, E. M. Santangelo, and R. Soldati, J. Phys. A **42**, 275401 (2009).

[22] L. Fritz, J. Schmalian, M. Müller, and S. Sachdev, Phys. Rev. B **78**, 085416 (2008).

[23] J. H. Davies, *The Physics of Low-Dimensional Semiconductors: An Introduction* (Cambridge Univesity Press, New York, 1998).

[24] S. P. Gavrilov and D. M. Gitman, Phys. Rev. D **53**, 7162 (1996); S. P. Kim and D. N. Page, *ibid.* **65**, 105002 (2002).

[25] A. Casher, H. Neuberger, and S. Nussinov, Phys. Rev. D **20**, 179 (1979).

[26] B. Dora and R. Moessner, Phys. Rev. B **81**, 165431 (2010).

[27] H. C. Kao, M. Lewkowicz, and B. Rosenstein, Phys. Rev. B **82**, 035406 (2010).

[28] B. Rosenstein, M. Lewkowicz, H. C. Kao, and Y. Korniyenko, Phys. Rev. B **81**, 041416(R) (2010).

[29] D. Allor, T. D. Cohen, and D. A. McGady, Phys. Rev. D **78**, 096009 (2008); T. D. Cohen and D. A. McGady, *ibid.* **78**, 036008, (2008).

[30] A. Barreiro, M. Lazzeri, J. Moser, F. Mauri, and A. Bachtold, Phys. Rev. Lett. **103**, 076601 (2009); N. Vandecasteele, A. Barreiro, M. Lazzeri, A. Bachtold, and F. Mauri, Phys. Rev. B **82**, 045416 (2010).

[31] E. B. Sonin, Phys. Rev. B **77**, 233408 (2008); **79**, 195438 (2009).

[32] A. Rycerz, P. Recher, and M. Wimmer, Phys. Rev. B **80**, 125417 (2009).

[33] E. Perfetto, G. Stefanucci, and M. Cini, Phys. Rev. B **82**, 035446 (2010).

[34] J. Schwinger, Phys. Rev. **82**, 664 (1951); G. Dunne and T. Hall, Phys. Rev. D **58**, 105022 (1998); S. P. Kim, H. K. Lee, and Y. Yoon, *ibid.* **78**, 105013 (2008).

[35] T. M. Rusin and W. Zawadzki, Phys. Rev. B **78**, 125419 (2008); **80**, 045416 (2009); F. T. Vasko, *ibid.* **82**, 245422 (2010).

[36] J. M. Dawlati, S. Shivaraman, M. Chandrasekhar, and F. Rana, Appl. Phys. Lett. **92**, 042116 (2008); D. Sun, Z. K. Wu, C. Divin, X. Li, C. Berger, W. A. de Heer, P. N. First, and T. B. Norris, Phys. Rev. Lett. **101**, 157402 (2008).

[37] V. Singh and M. M. Deshmukh, Phys. Rev. B **80**, 081404(R) (2009).

[38] D. Patanè, L. Amico, A. Silva, R. Fazio, and G. E. Santoro, Phys. Rev. B **80**, 024302 (2009).

[39] R. R. Nair, P. Blake, A. N. Grigorenko, K. S. Novoselov, T. J. Booth, T. Stauber, N. M. R. Peres, and A. K. Geim, Science **320**, 1308 (2008); K. F. Mak, M. Y. Sfeir, Y. Wu, C. H. Lui, J. A. Misewich, and T. F. Heinz, Phys. Rev. Lett. **101**, 196405 (2008).

[40] A. Onipko, Phys. Rev. B **78**, 245412 (2008).

[41] B. A. Bernevig, T. L. Hughes, and S-C. Zhang, Science **314**, 1757 (2006); X.-L. Qi and S.-C. Zhang, Phys. Today **63**, 33 (2010); C. Brüne, A. Roth, E. G. Novik, M. König, H. Buhmann, E. M. Hankiewicz, W. Hanke, J. Sinova, and L. W. Molenkamp, Nat. Phys. **6**, 448 (2010); L. B. Zhang, K. Chang, X. C. Xie, H. Buhmann, and L. W. Molenkamp, New J. Phys. **12**, 083058 (2010).